SUBJECT TO LARGE TEMPERATURE GRADIENT

S.A. Suslov

Department of Mathematics and Computing,
University of Southern Queensland, Toowoomba, Queensland 4350, Australia
e-mail: ssuslov@usq.edu.au

Mixed convection flows in a two-dimensional vertical channel have been the subject of intensive study for the last few decades, see works by Rudakov [4] and Fukui et al [2] just to name a few. Typically the approach taken to analyse the resulting flow uses the Boussinesq approximation of the Navier-Stokes equations which assumes no fluid properties variations except a linear density dependence on the temperature in the buoyancy term. The resulting solutions are relatively simple and can frequently be found analytically. But such an approach is valid only if the maximum temperature difference in the flow region does not exceed a few degrees Kelvin. This limitation is too restrictive for many practical applications such as chemical vapour deposition reactors. In this work Low-Mach-Number (LMN) equations [1] are used to account for realistic fluid property variations leading to a rich variety of flow instabilities in mixed convection between two differentially heated vertical walls.

Consider a flow of air with the average (reference) temperature $T_r = 300K$ whose density ρ, dynamic viscosity μ, thermal conductivity k and specific heat c_p nondimensionalised with respect to their values at T_r vary with temperature T according to the ideal gas and Sutherland formulae

$$\rho T = 1, \quad \mu = T^{3/2}\frac{1.368}{T+0.368}, \quad k = T^{3/2}\frac{1.648}{T+0.648}, \quad c_p = 1 \tag{1}$$

between two isothermal vertical plates separated by the gap of width H and maintained at different temperatures T_h and T_c, $T_h > T_c$. As discussed in [5] such flow is described by the LMN equations

$$\frac{\partial \rho}{\partial t} + \frac{\partial \rho u_i}{\partial x_i} = 0\,, \tag{2}$$

$$\frac{\partial \rho u_i}{\partial t} + \frac{\partial \rho u_i u_j}{\partial x_j} = -\frac{\partial \Pi}{\partial x_i} + \frac{Gr}{2\epsilon}(\rho - 1)n_i + \frac{\partial \tau_{ij}}{\partial x_j} \tag{3}$$

$$\rho c_p\left(\frac{\partial T}{\partial t} + u_j\frac{\partial T}{\partial x_j}\right) = \frac{1}{Pr}\frac{\partial}{\partial x_j}\left(k\frac{\partial T}{\partial x_j}\right)\,, \tag{4}$$

where the Grashof (buoyancy effects), Reynolds (applied pressure gradient effects) and Prandtl numbers and non-dimensional temperature difference between the walls (property variations effects) are defined using the reference values:

$$Gr = \frac{\rho_r^2 g(T_h - T_c)H^3}{\mu_r^2 T_r},\ Re = -\frac{\rho_r H^3}{12\mu_r^2}\frac{d\Pi}{dy},\ Pr = \frac{\mu_r c_{pr}}{k_r} = 0.71\,,\ \epsilon = \frac{T_h - T_c}{2T_r}\,.$$

We investigate in detail the structure of mixed convection flow as parameter ϵ varies from $\epsilon \to 0$ (Boussinesq limit of zero temperature variation across the channel) to $\epsilon = 0.6$ (strongly non-Boussinesq regime with the temperature difference of $\Delta T = 360K$ between the walls).

The steady y-independent parallel basic flow profiles which can exist in a channel of large aspect ratio $A > 20$ are shown in Figure 1. Since both the viscosity and thermal conductivity decrease with temperature, the flow can accommodate larger gradients near the cold wall, and so both velocity and temperature profiles shift towards it. The fluid property variations have a noticeable influence on the flow: the temperature deviates from

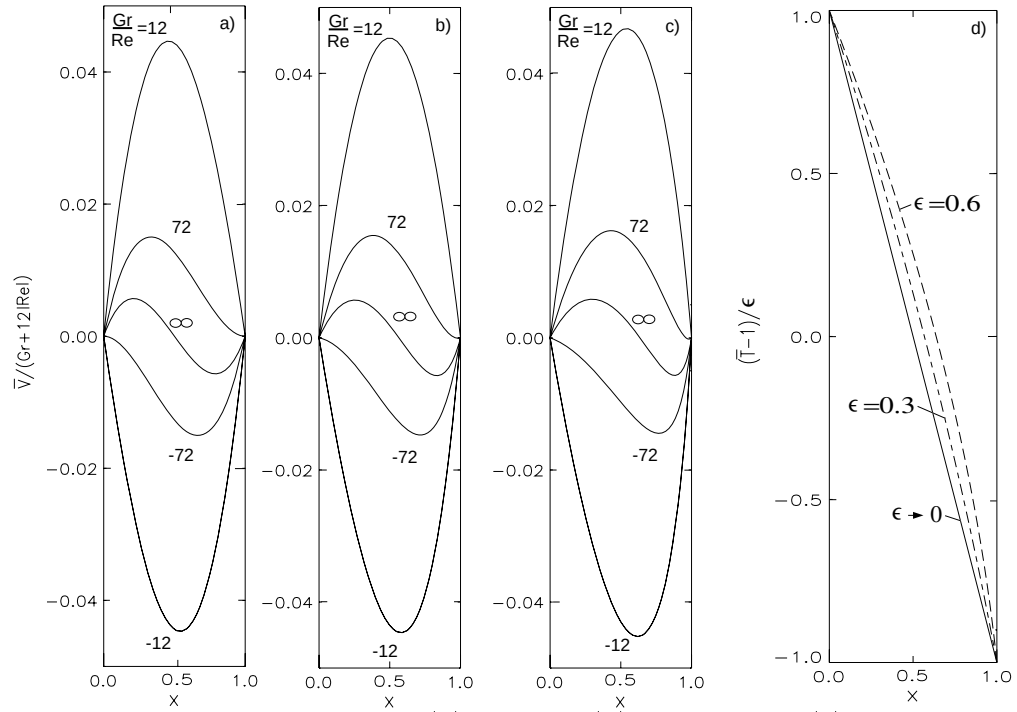

Figure 1: Basic flow velocity for $\epsilon \to 0$ (a), $\epsilon = 0.3$ (b) and $\epsilon = 0.6$ (c) and temperature (d) profiles.

a classical Boussinesq linear profile and the velocity distributions lose all its symmetries. In particular, $v(x, Re, Gr) \neq v(-x, -Re, Gr)$ i.e. changing the direction of the applied pressure gradient leads to nontrivial changes in the basic flow velocity fields. For this reason spatio-temporal instability results will be presented for both positive and negative values of the Reynolds number (except when $\epsilon \to 0$).

Detailed linear stability analysis conducted in [5] revealed a number of new features never found previously due to the limitations of the Boussinesq approximation. Firstly, the variation of the transport fluid properties with temperature generally leads to stabilisation of basic flow. This is because the large gradient regions where the instabilities normally occur shift towards the (cold) wall where the disturbance damping effects are stronger. Secondly, the instabilities are found to be oscillatory for *any* finite value of ϵ even for $Re = 0$. The disturbance wave speed is predominantly downwards. This is again because the large gradient regions generating instability are shifted towards the cold wall where the local flow velocity is negative, see Figure 1. Thirdly, an additional nonlinearity associated with realistic fluid property variations leads to the appearance of new physically distinct instability modes not found in Boussinesq flows. A weakly nonlinear analysis presented in [7] showed that the instabilities detected in Boussinesq and weakly non-Boussinesq flows at moderate values of the Reynolds number are caused by the shear of the flow. These instabilities appearing near the inflection point of the basic flow velocity profile tend to decrease the overall flow gradients via cross-channel mixing. In contrast, the new instability arising at large values of ϵ appear only near the cold wall where it enhances downward motion. This is caused by lumps of overcooled fluid with lower viscosity and thermal conductivity but having larger density, which literally slide down the cold wall (see Figure 2). This instability is caused by the buoyancy. It has a very distinct spatial structure with large wavelength and large negative wave speed. Thus one of the major roles the non-Boussinesq fluid property variations play is breaking the symmetry and introducing the preferred propagation direction. In turn this makes analysis of the spatio-temporal dynamics of localised disturbance packets in unstable mixed convection flows an interesting and non-trivial task.

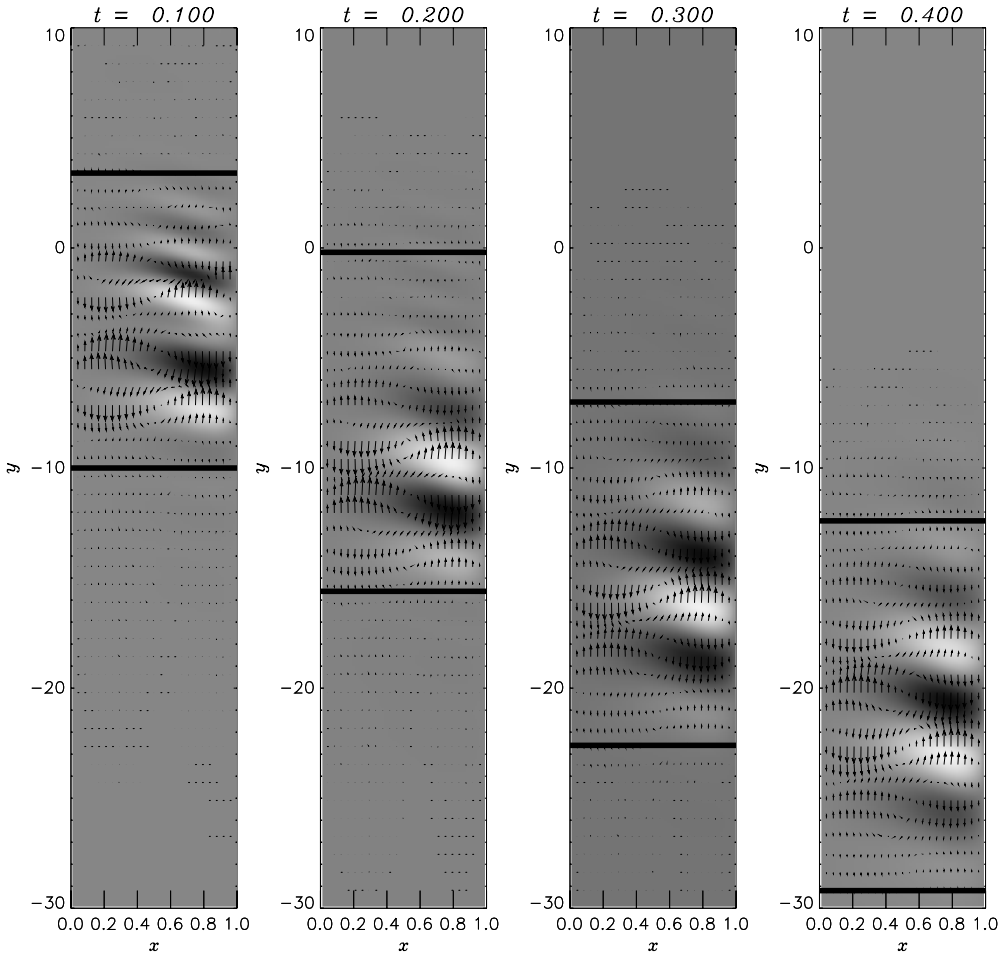

Figure 2: (a) Evolution of convectively unstable buoyancy instability mode at $(Re, Gr, \epsilon) = (0, 10000, 0.6)$. Grey shades represent the disturbance thermal field.

Spatio-temporal dynamics of localised disturbances

Localised unstable disturbance envelopes in a dispersive medium can grow in amplitude, be carried away by the primary flow and can extend in the direction of this flow. A combination of these three major dynamics leads to two distinct overall scenarios referred to as convective and absolute instabilities. They are illustrated in Figures 2 and 3, respectively, which are obtained by direct numerical integration of the linearised disturbance equations in the Fourier space (inverse Fourier transform). The group speed of a convectively unstable disturbance envelope is large in comparison with its extension rate and the localised disturbances, while growing in a moving frame of reference, are carried by the basic flow away from any stationary position leaving an undisturbed field behind. In contrast, when the instability is absolute the envelope extension rate is sufficiently large so that the envelope edges move in the opposite directions. In this case disturbances will eventually occupy the complete flow region. The mathematical details of determining the character of instability are too lengthy to be given here and can be found, for example, in [3] and references therein. Note that although the theory of spatio-temporal instabilities is well understood nowadays, a robust numerical procedure automatically and accurately determining the transition between multi-mode absolute and convective instabilities in multi-parameter physical problems is still not widely available. Such a methodology has been recently developed by the author and will be reported in upcoming full length publications. Here we only have space to report the major

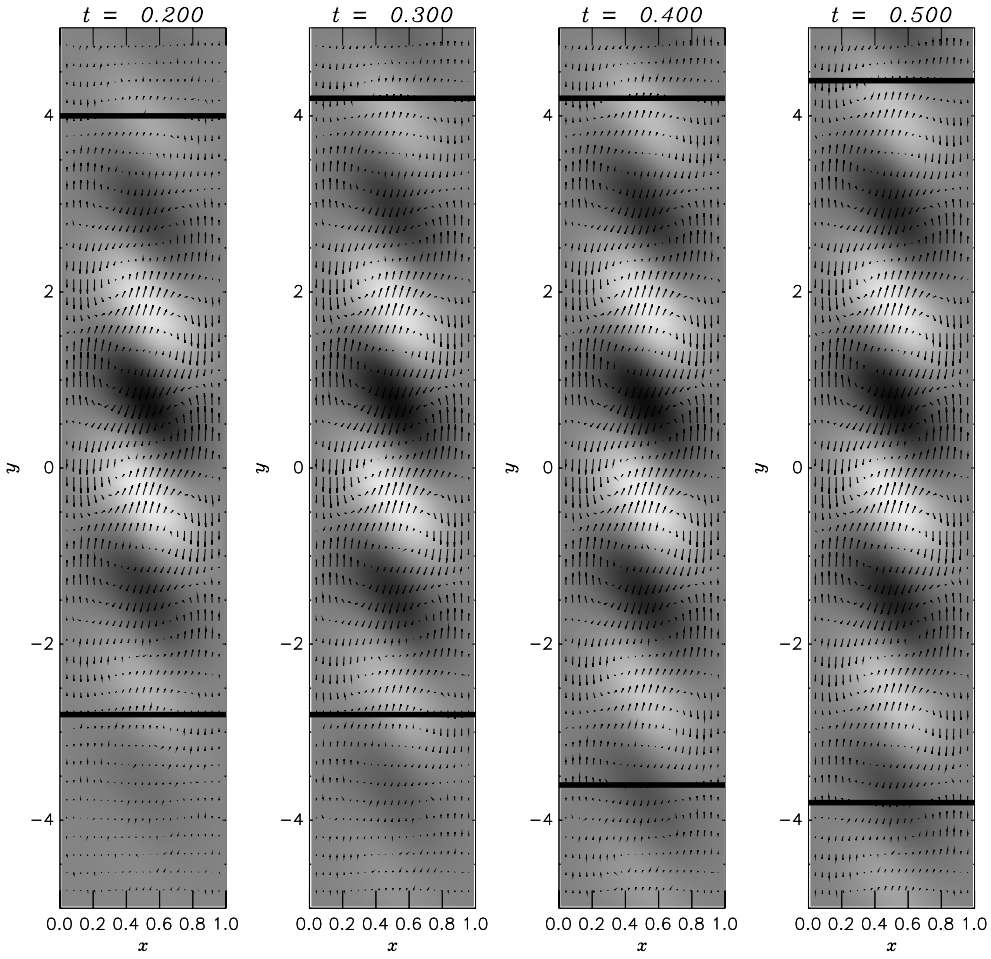

Figure 3: (a) Evolution of absolutely unstable shear instability mode at $(Re, Gr, \epsilon) = (0, 8100, 0.005)$. Grey shades represent the disturbance thermal field.

physical results of this comprehensive and extremely demanding numerical investigation.

The classical Boussinesq result for natural convection in the considered geometry is that the linear instability is stationary [4] and, consequently, absolute. This remains true only for very small temperature differences between the walls: as seen from Figure 3 even for $\Delta T = 3K$ the preferred propagation direction exists. Still the group speed is so small that the instability observed near the centre of the channel (velocity inflection point) is absolute. At the same time any finite pressure gradient applied along the channel leads to a non-zero group speed of the disturbance envelop which is faster than the envelope extension rate. Thus it is found that the linear (shear) instability observed in mixed convection in Boussinesq regimes is always convective with the disturbance propagation direction determined by the direction of the applied longitudinal pressure gradient. For any fixed pressure gradient (Re) transition to absolute instability occurs at $Gr > Gr_c$, where Gr_c is the linearly critical Grashof number. The physical reason for this is that in order to support the propagation of disturbances in both directions regardless of the applied longitudinal pressure gradient the basic flow should have a cubic-like (in contrast to parabolic) profile which requires a sufficiently large value of the Gr/Re ratio, see Figure 1. Because of this the value of the Grashof number for which the transition to absolute instability occurs increases rapidly with Re. Only for $Re = 0$ the linear instability coincides with absolute. A complete stability diagram is presented in Figure 4 (a) (the diagram for $Re < 0$ is a mirror reflection of that for $Re > 0$ and is not shown).

The instability diagram changes dramatically with increasing ϵ when non-Boussinesq fluid property variations start playing a significant symmetry-breaking role. Diagram 4 (b) shows that, similar to the Boussinesq limit, linear instability in weakly non-Boussinesq convection is always convective with absolute instability kicking in at significantly larger values of Gr. It is interesting to note that the linear instability is absolute at a single point of $Re \approx 1.19$. This means that in contrast to the Boussinesq limit the linear instability observed in purely natural convection ($Re = 0$) under non-Boussinesq conditions is convective. Only when a small but finite longitudinal pressure gradient driving the flow upwards is applied, then it becomes absolute (the disturbance group speed vanishes indicating the transition). Physically this is due to the symmetry breaking effects of the fluid property variations: the non-Boussinesq natural convection is characterised by a small negative overall mass flux. An external pressure gradient has to be applied to compensate for this asymmetry and make the mass flux zero. This is directly related to the direction of the disturbance propagation and in turn determines the character of linear instability. Note also the significant asymmetry between the stability diagrams for $Re \lessgtr 0$ in Figure 4 (b): the basic flow is substantially more stable if the applied pressure gradient supports the downward flow (in the direction of gravity) because in this case the velocity gradient of a primary flow is smaller.

The stability diagram for a strongly non-Boussinesq regimes becomes progressively more complicated because two physically distinct (shear- and buoyancy-driven) instabilities may be present in the flow simultaneously, see [5] for detail. This leads to a diagram which includes at least 10 regions with qualitatively distinct instability dynamics. They are described in detail in [8] and here we limit ourselves to the discussion of the most important multi-mode instability features.

If the applied pressure gradient is relatively weak ($|Re| \sim 0$) the flow first becomes unstable due to the buoyancy disturbances which have a preferred downward propagation direction regardless of the sign of the Reynolds number. The typical dynamics of a buoyancy disturbance is shown in Figure 2. This situation corresponds to a convectively unstable regime as the disturbance wave envelope (bounded by the two horizontal lines between which the thermal disturbance magnitude is above a specified fixed level) propagates away from its original location. Only when the pressure gradient opposing this motion becomes sufficiently strong ($Re \gtrsim 594$) is it capable of pushing the buoyancy instability cells upwards and the buoyancy instability becomes absolute. For smaller values of Re the buoyancy instability remains convective for all Gr. The shear mode also becomes convectively unstable first, but in contrast to the buoyancy one it always experiences transition to absolute instability for sufficiently large values of Gr. This is because increasing the Grashof number leads to a basic flow reversal which supports disturbance propagation in both directions. This is required for absolute instability. In contrast, increasing the Reynolds number (pressure gradient) leads to a unidirectional basic flow (see Figure 1) and increases its tendency to become convectively unstable.

An interesting situation is observed in the regions denoted by CAI in Figure 4 (c). Here one of the modes (typically buoyancy) is still convectively unstable while the other (shear) is already absolutely unstable. In this situation only the dominant absolute (shear) instability is expected to be observed in practise at large times because convectively unstable (buoyancy) disturbances will be carried away. At the same time the nonlinear interaction of the two modes is expected to produce an even richer variety of flow patterns, but this is left for future study.

In summary, the nonlinear fluid property variations associated with large temperature differences in the flow region are shown to lead to a remarkably rich variety of spatio-temporal instabilities observed even in very simple geometries. The analysis of these instabilities requires careful analytical and elaborate numerical investigations whose full detail will be

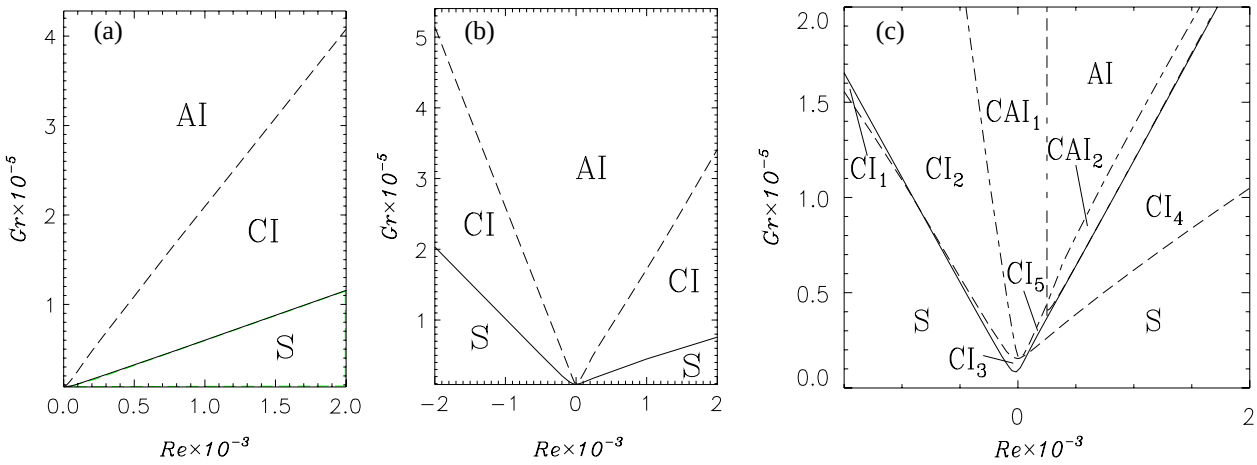

Figure 4: Linear (solid lines) and absolute (dashed lines) instability boundaries for (a) $\epsilon \to 0$, (b) $\epsilon = 0.3$ and (c) $\epsilon = 0.6$. The letters denote various parameter regions: S—stability, CI—convective instability, AI—absolute instability, CAI—mixed multi-mode convective/absolute instability.

reported by the author elsewhere. The problem discussed offers significant academic interest enhanced by its direct relevance to industrial applications such as chemical vapour deposition reactors and thermal insulation systems.

References

[1] D.R. Chenoweth and S. Paolucci, Gas flow in vertical slots with large horizontal temperature differences, *Phys. Fluids*, **28**, 2365–2374, 1985.

[2] K. Fukui, M. Nakajima, H. Ueda and T. Mizushina, Flow instability and transport phenomena in combined free and forced convection between vertical parallel plates, *J. Chem. Engng Japan*, **15**, 172–180, 1982.

[3] P. Huerre and P.A. Monkewitz, Local and global instabilities in spatially developing flows, *Ann. Rev. Fluid Mech.*, **22**, 473–537, 1990.

[4] R.N. Rudakov, Spectrum of perturbations and stability of convective motion between vertical plates, *Appl. Math. Mech.*, **31**, 376–383, 1967.

[5] S.A. Suslov and S. Paolucci, Stability of mixed-convection flow in a tall vertical channel under non-Boussinesq conditions, *J. Fluid Mech.*, **302**, 91–115, 1995.

[6] S.A. Suslov and S. Paolucci, Nonlinear stability of mixed convection flow under non-Boussinesq conditions. Part 1. Analysis and bifurcations, *J. Fluid Mech.*, **398**, 61–85, 1997.

[7] S.A. Suslov and S. Paolucci, Nonlinear stability of mixed convection flow under non-Boussinesq conditions. Part 2. Mean flow characteristics, *J. Fluid Mech.*, **398**, 87–108, 1997.

[8] S.A. Suslov, Multi-mode spatio-temporal instability in non Boussinesq convection, to appear in *J. Aus. Math. Soc. E*, 2003.